














Arctic mercury flux increased through the Last Glacial Termination with a warming climate

Received: 14 April 2022

Accepted: 23 March 2023

Published online: 04 May 2023

 Check for updates

Delia Segato ^{1,2}, Alfonso Saiz-Lopez ✉³, Anoop Sharad Mahajan ⁴, Feiyue Wang ⁵, Juan Pablo Corella ^{3,6}, Carlos Alberto Cuevas ³, Tobias Erhardt ^{7,8}, Camilla Marie Jensen⁸, Chantal Zeppenfeld ⁸, Helle Astrid Kjær ⁹, Clara Turetta ^{1,2}, Warren Raymond Lee Cairns ^{1,2}, Carlo Barbante ^{1,2} & Andrea Spolaor ^{1,2}✉

Mercury is a pollutant of global concern, especially in the Arctic, where high levels are found in biota despite its remote location. Mercury is transported to the Arctic via atmospheric, oceanic and riverine long-range pathways, where it accumulates in aquatic and terrestrial ecosystems. While present-day mercury deposition in the Arctic from natural and anthropogenic emissions is extensively studied, the control of past climate changes on natural mercury variability remains unknown. Here we present an Arctic mercury record covering the Last Glacial Termination to the early Holocene epoch (15.7–9.0 thousand years before 2000 CE), collected as part of the East Greenland Ice-Core Project. We find a threefold increase in mercury depositional fluxes from the Last Glacial Termination into the early Holocene, which coincided with abrupt regional climate warming. Atmospheric chemistry modelling, combined with available sea-ice proxies, indicates that oceanic mercury evaporation and atmospheric bromine drove the increase in mercury flux during this climatic transition. Our results suggest that environmental changes associated with climate warming may contribute to increasing mercury levels in Arctic ecosystems.

Mercury (Hg) is a naturally occurring pollutant of global concern due to its well-documented negative impact on both human and ecosystem health^{1,2}. From this perspective, the Arctic region is of particular concern since the complex biogeochemical cycle of Hg results in elevated concentrations found in Arctic marine mammals, threatening the health of Inuit and other Indigenous peoples who rely on these

animals as a food source³. Hg is released into the atmosphere through natural and anthropogenic processes. Its emissions increased globally with the Industrial Revolution and peaked at around the 1970s⁴. Since then, atmospheric Hg concentration has slightly decreased, thanks to regional and global initiatives to control anthropogenic Hg emission such as the recently enforced Minamata Convention⁵.

¹Institute of Polar Sciences, CNR-ISP, Campus Scientifico Via Torino, Venice-Mestre, Italy. ²Department of Environmental Sciences, Informatics and Statistics, University Ca' Foscari of Venice, Venice-Mestre, Italy. ³Department of Atmospheric Chemistry and Climate, Institute of Physical Chemistry Rocasolano, CSIC, Madrid, Spain. ⁴Indian Institute of Tropical Meteorology, Ministry of Earth Sciences, Pune, India. ⁵Centre for Earth Observation Science, and Department of Environment and Geography, University of Manitoba, Winnipeg, Manitoba, Canada. ⁶Department of the Environment (DMA), CIEMAT, Madrid, Spain. ⁷Alfred Wegener Institute, Helmholtz Centre for Polar and Marine Research, Bremerhaven, Germany. ⁸Climate and Environmental Physics, Physics Institute and Oeschger Center for Climate Change Research, University of Bern, Bern, Switzerland. ⁹Physics of Ice, Climate and Earth, Niels Bohr Institute, University of Copenhagen, Copenhagen, Denmark. ✉e-mail: a.saiz@csic.es; andrea.spolaor@cnr.it

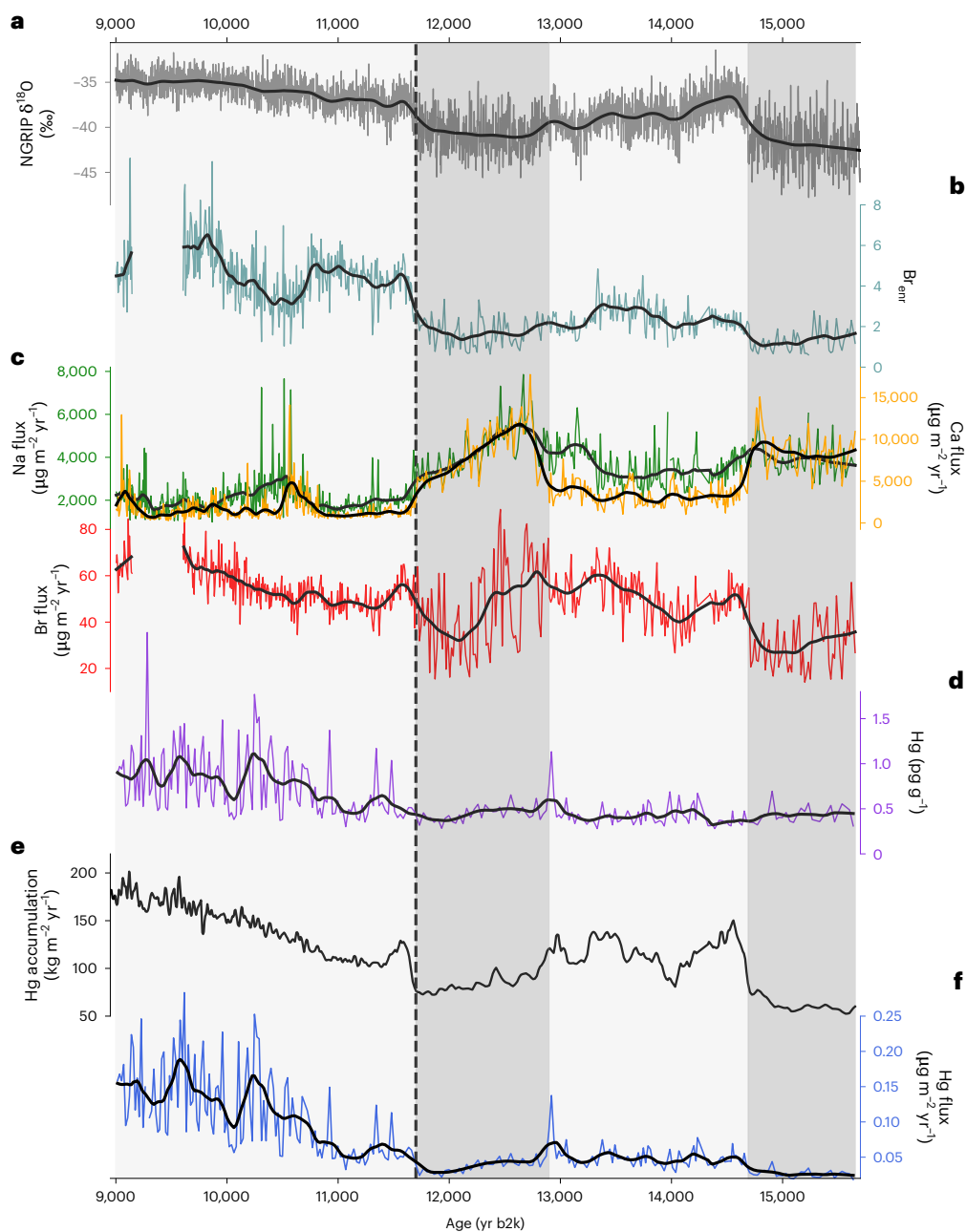


Fig. 1 | EGRIP Hg, Br, Na and Ca fluxes, Hg concentration, accumulation profile and NGRIP $\delta^{18}\text{O}$ for the period 9.0–15.7 kyr b2k. **a**, NGRIP $\delta^{18}\text{O}$ (‰) (ref. 55), used here as a proxy of local temperature. **b**, EGRIP Br_{ent} , indicator of first-year sea-ice variability. **c**, EGRIP Na, Ca and Br fluxes ($\mu\text{g m}^{-2} \text{yr}^{-1}$). **d**, Hg concentration (pg g^{-1}). **e**, Hg accumulation ($\text{kg m}^{-2} \text{yr}^{-1}$ in water equivalent) (ref. 56).

f, Hg flux ($\mu\text{g m}^{-2} \text{yr}^{-1}$). Darker-colour shading indicates the colder periods of the Younger Dryas (11.7–12.9 kyr b2k) and Oldest Dryas (>14.7 kyr b2k); lighter-colour shading indicates warmer periods of the early Holocene (9.0–11.7 kyr b2k) and Bølling-Allerød (12.9–14.7 kyr b2k). The dashed line indicates the Holocene–Glacial transition 11.7 kyr b2k.

The major global Hg reservoirs include, in increasing order, the atmosphere, terrestrial environments (particularly soils) and the ocean^{6,7}. Most of the atmospheric Hg deposited in terrestrial compartments is retained in humus-rich upper soils and bound to organic matter⁸. By contrast, a large fraction of the atmospheric mercury deposited in the ocean is volatilized back to the atmosphere, driven by photochemical and biological processes^{9,10}. The fraction of Hg that is not evaded to the atmosphere is scavenged by organic particles and ultimately deposited in marine sediments^{10,11}.

The dominant form of Hg in the atmosphere is gaseous elemental mercury (Hg^0) with a lifetime of 3–6 months, allowing its long-distance transport¹². In the Arctic, reactive bromine (Br) emitted from the surface

of seasonal sea ice during spring, known as bromine explosion events, oxidizes gaseous elemental mercury to gaseous oxidized mercury (mainly Hg(II) compounds including HgBr_2). Gaseous oxidized mercury is readily deposited on snow and ice surfaces, close to the bromine emission sources¹³, resulting in atmospheric mercury depletion events. A large fraction of the Hg(II) deposited during mercury depletion events is rapidly photo-reduced and re-emitted to the atmosphere⁷. The remaining Hg enters the ocean and can be methylated to methylmercury¹⁴, which is highly bio-accumulative, biomagnifying and toxic, posing a health risk to marine mammals and Indigenous peoples³.

Palaeoclimatic archives (such as tree rings, peat, marine and lacustrine sediments, coral skeletons and ice cores) have been widely used

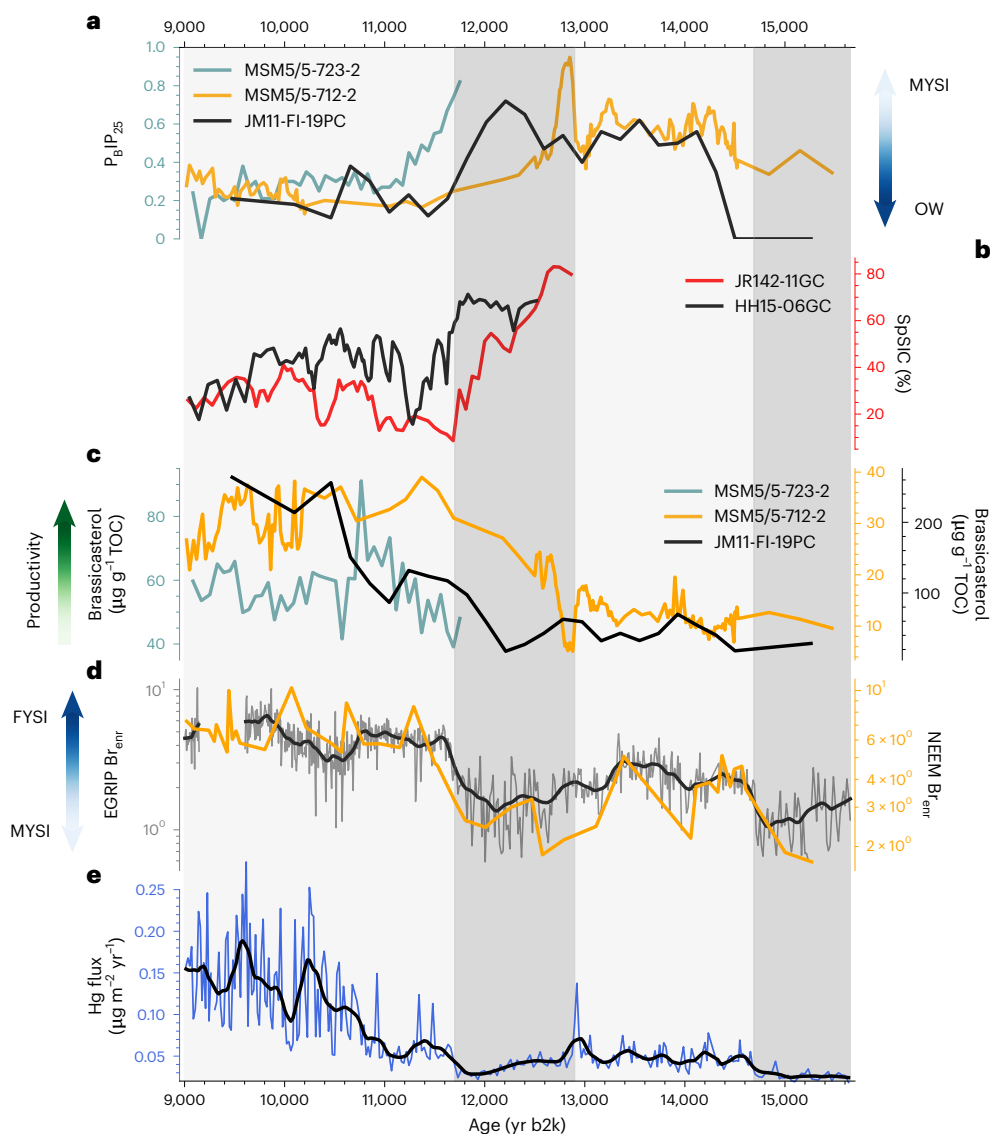


Fig. 2 | EGRIP Hg and proxies of sea-ice variability. **a**, Cores MSM05/5_723-2 $P_{BIP_{25}}$ ²⁸, MSM05/5_712-2 $P_{BIP_{25}}$ ²⁷ and JM11-FI-19PC $P_{BIP_{25}}$ ³⁰. **b**, Reconstructed spring sea-ice concentrations (SpSIC %) from JR142-11GC and HH15-06GC cores⁴⁴. **c**, MSM05/5_723-2 brassicasterol ($\mu\text{g g}^{-1}$ total organic carbon (TOC))²⁸, MSM05/5_712-2 brassicasterol ($\mu\text{g g}^{-1}$ TOC)²⁷ and JM11-FI-19PC brassicasterol ($\mu\text{g g}^{-1}$ TOC)³⁰. **d**, EGRIP Br_{enr} (this study) and North Greenland Eemian (NEMEM)

Br_{enr} ³¹. **e**, EGRIP Hg flux ($\mu\text{g m}^{-2} \text{yr}^{-1}$). Darker-colour shading indicates the colder periods of the Younger Dryas (11.7–12.9 kyr b2k) and Oldest Dryas (>14.7 kyr b2k); lighter-colour shading indicates warmer periods of the early Holocene (9.0–11.7 kyr b2k) and Bølling–Allerød (12.9–14.7 kyr b2k). $P_{BIP_{25}}$ is a sea-ice proxy showing values close to 1 for MYSI and close to 0 for open water (OW). Conversely, Br_{enr} indicates FYSI when levels are higher and MYSI when levels are lower.

to reconstruct the recent history of atmospheric Hg^{15–17}. Hg reconstructions from Antarctica¹⁷, South America^{18–20} and Switzerland²¹ extend beyond the Last Glacial Termination (LGT), the period that includes the dramatic climate transition from the last glaciation to the Holocene epoch. Most Hg records from the Arctic investigate the Industrial Period, and only a few extend to the past millennia^{22–26}. These records have a low temporal resolution and cover a period when anthropogenic activities influenced Hg emissions. To cover this knowledge gap, we present an Arctic record of mercury that covers the Last Glacial Termination and the early Holocene (9.0–15.7 kyr before 2000 CE (b2k)). Mercury was measured with a high temporal resolution in the East Greenland Ice Project (EGRIP) ice core retrieved from the Greenland Ice Sheet. The transition from the LGT to the Holocene is a perfect context for investigating how the Arctic Hg biogeochemical cycle changes in response to abrupt climate shifts. By combining an atmospheric Hg model and proxies from marine sediments and ice cores^{27–31}, we uncover

the likely drivers of Hg variability in the Arctic in the context of past climatic changes and with no anthropogenic influence.

Ice-core measurements

Low mercury concentrations are found at the LGT until 11 kyr b2k (0.4 ± 0.1 (1σ) pg g^{-1}), while in the early Holocene, Hg concentrations double (0.8 ± 0.4 (1σ) pg g^{-1}) (Fig. 1), concomitant with an increase of -10°C in Greenland as inferred from North Greenland Ice-Core Project (NGRIP) $\delta^{18}\text{O}$ and $\delta^{15}\text{N}$ (ref. 32). Average Hg fluxes are 118 ± 65 (1σ) $\text{ng m}^{-2} \text{yr}^{-1}$ in the early Holocene (9.0–11.7 kyr b2k) and 49 ± 15 (1σ) $\text{ng m}^{-2} \text{yr}^{-1}$ in the Bølling–Allerød (12.9–14.7 kyr b2k); these fluxes are substantially higher than those in colder periods, that is, the Younger Dryas (39 ± 12 (1σ) $\text{ng m}^{-2} \text{yr}^{-1}$, 11.7–12.9 kyr b2k) and the last millennium of the Oldest Dryas (27 ± 5 (1σ) $\text{ng m}^{-2} \text{yr}^{-1}$, 14.7–15.7 kyr b2k).

In addition to Hg, we determined Br, sodium (Na), and calcium (Ca) fluxes in the EGRIP core (Fig. 1). All records exhibit millennial-scale

variability, in parallel with local temperature changes, as inferred from NGRIP $\delta^{18}\text{O}$ (Fig. 2). Like that of Hg, the Br flux shows lower and highly variable levels during the Younger Dryas (47 ± 19 (1σ) $\text{ng m}^{-2} \text{yr}^{-1}$) and Oldest Dryas (27 ± 5 (1σ) $\text{ng m}^{-2} \text{yr}^{-1}$) and higher values (55 ± 8 (1σ) $\text{ng m}^{-2} \text{yr}^{-1}$) during warm periods. By contrast, Na and Ca fluxes show the opposite behaviour, with values two to five times higher in the Younger Dryas compared with the early Holocene as a result of drier climate and stronger winds prevalent during colder periods³³. We have also derived the Br enrichment (Br_{enr}) record (Methods and Fig. 2), known to be a tracer of first-year sea ice (FYSI)^{34,35}. The value of Br_{enr} is low during colder periods, with an average value of 1.3 ± 0.5 (1σ) and higher during warmer periods with an average value of 4.5 ± 1.4 (1σ) in the early Holocene, similar to what was observed in the North Greenland Eemian ice core³¹.

Mercury increase through the Glacial to Holocene transition

At the transition from the LGT to the Holocene, the climate warming led to drastic environmental changes in the Arctic, resulting in a threefold increase in Hg depositional flux. To investigate the likely causes of this marked change, we use an atmospheric Hg chemistry model (Methods and Supplementary Information section 5) to estimate the relative influence of different environmental conditions and natural Hg sources on the EGRIP Hg flux. We combine the model with marine and ice-core observations to assess the main drivers that might have contributed to this strong variability as a result of the interplay between (1) Hg emissions affected by the variability in sea-ice cover and open-ocean conditions; (2) atmospheric Hg chemistry, including reactions with Br (Methods), which is the main atmospheric Hg oxidizer and is sensitive to the sea-ice dynamics³⁶; and (3) atmospheric transport, the influence of winds and Hg uptake on mineral dust and other aerosols¹⁷. Possible competitive processes that can affect the Hg signal, such as changes in snow accumulation, post-depositional processes and volcanic events, are discussed in Supplementary Information section 3.

One of the primary natural sources of Hg in the atmosphere is Hg evasion driven by biological and photochemical processes³⁷. In aquatic ecosystems, phototrophic and chemotrophic organisms reduce Hg(II) to volatile Hg^0 as a detoxification mechanism. Mercury is also reduced at the ocean surface by photochemical reactions³⁸. Soerensen et al.³⁹ estimated that, in the Arctic, gaseous Hg evasion accounts for 44% of total Hg removal pathways from the ice-free water column. The presence of multi-year sea ice (MYSI) strongly limits the ocean–atmosphere exchange of Hg, as well as primary productivity and light penetration to the ocean surface, that would promote Hg(II) reduction^{39–41}, while in areas with open ocean and/or FYSI, Hg^0 is easily volatilized from the ocean surface.

EGRIP Br_{enr} , a tracer of sea-ice variability, shows higher values during the warmer periods of our record, indicating a large seasonal amplitude in sea-ice cover in the EGRIP source area and probably more open water during the summer months. Using back-trajectory analysis (Supplementary Information section 2), we find that ocean and/or sea-ice areas potentially influencing the EGRIP site are located both on the western (Baffin Bay and Labrador Sea) and eastern (Greenland Sea and Fram Strait area) sides of Greenland, as well as the Southern part of the Arctic Ocean. These ocean areas were mostly covered by extensive sea ice during the Last Glacial Maximum. For the following millennia, increasing solar radiation led to MYSI break-up in the sub-polar North Atlantic during the last deglaciation^{27,29–31}, interrupted 12.9 kyr ago by the Younger Dryas cold spell. The Younger Dryas was a millennium-long period of cooler climate caused by freshwater discharge from Lake Agassiz and the Canadian Arctic. Extensive sea-ice conditions and increased export through the Fram Strait during this period were associated with weaker Atlantic meridional overturning circulation and inhibited deep water formation in the sub-polar North Atlantic⁴². At the onset of the Holocene, MYSI reduced in extent and

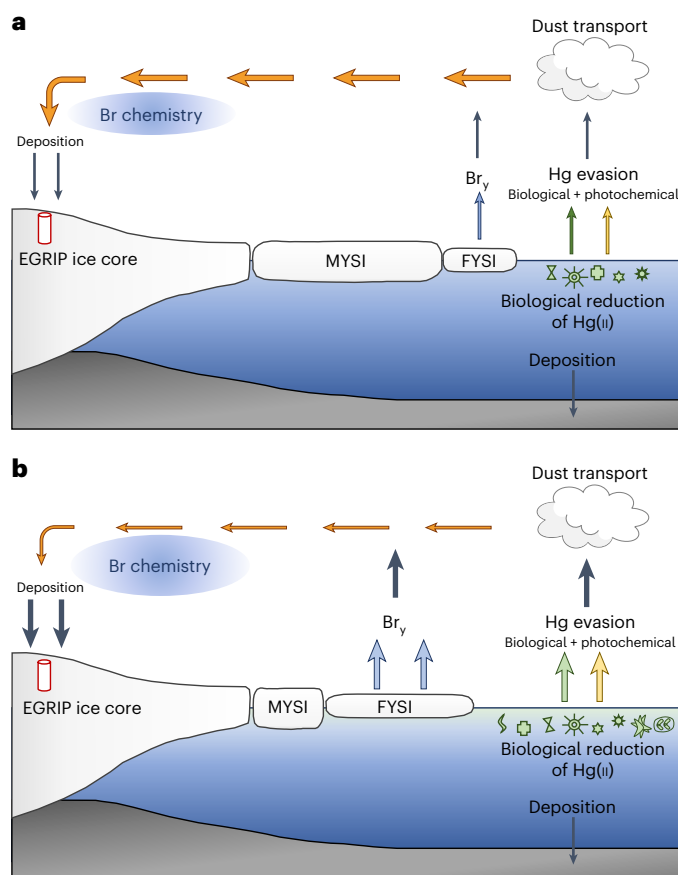


Fig. 3 | Schematic representation of the differences in mercury emission, transport, chemistry and deposition during the LGT and the early Holocene. **a**, LGT (11.0–15.7 kyr b2k). The dust transport towards the Greenland Ice Sheet is stronger, while Hg oceanic evasion, as well as reactive Br (Br_y) emission from FYSI and atmospheric Br chemistry are weaker. The overall result is low Hg deposition. **b**, Early Holocene (9.0–11.7 kyr b2k). The opposite condition: weak wind transport, strong Hg evasion due to reduced extension of MYSI, higher emission of Br, from more-extensive FYSI and, consequently, stronger atmospheric Br chemistry. The early Holocene scenario results in enhanced Hg deposition.

the Atlantic meridional overturning circulation reinvigorated with consequent enhanced flow of North Atlantic waters to high latitudes⁴³. The MYSI melting increased open-ocean surface availability for Hg evasion and increased the seasonal formation of FYSI in the sub-polar North Atlantic, as inferred from a drop in PIP_{25} , a biomarker associated with diatoms living in sea ice, in the sediment cores from the Fram Strait^{27,28} and the Norwegian Sea³⁰ (Fig. 2) and the increased Br_{enr} in the record presented here. Reduced sea-ice conditions at the onset of the Holocene are found in the northern Barents Sea, indicated by open-water phytoplankton biomarkers⁴⁴. Ice-free summers were reached at 10.6 kyr, with sea surface temperatures up to 6°C in the Fram Strait area²⁸. In response to a reduced or thin sea-ice cover, higher content of the phytoplankton-derived biomarkers brassicasterol^{27,28,30} and highly branched isoprenoid⁴⁴ found in the mentioned sediment cores, indicate favourable conditions for phytoplankton growth and primary productivity in general. On the western side of Greenland, instead, at the onset of the Holocene, MYSI disappeared progressively, and annual productivity increased starting from the Labrador Sea, while the Baffin Bay was covered by quasi-perennial sea ice until 7.4 kyr b2k²⁹. MYSI decline, increase in primary productivity and light penetration at the ocean surface were some of the consequences of climate warming. During this time, Greenland Ice Sheet meltwater might have increased Hg input to the sub-polar North Atlantic and Arctic Ocean^{39,45}.

These conditions, together, probably have a large influence on the Hg biogeochemical cycle, leading to higher oceanic Hg evasion from the ocean due to biological and photochemical processes. Although biological activity acts as a sink of Hg to the deep ocean sediments, our results indicate that the increase in primary productivity and the resulting Hg evasion due to retreat of MYSI more than compensates this effect.

Previous work⁴⁶ attributed elevated Hg concentrations at Dome C, Antarctica, during the Last Glacial Maximum to higher palaeoproductivity in upwelling and subpolar areas. Thus, the generally larger fraction of open ocean in the early Holocene was probably one of the drivers of the higher levels of Hg recorded at EGRIP (Fig. 3). Our model results show that if only Hg emission was responsible for the enhancement in the ice core, then the atmospheric Hg should have increased by ten times, or the Hg evasion should have decreased by a similar fraction during the Holocene with respect to the Younger Dryas (simulation number 8 in Supplementary Table 3). Such enhancement is comparable to reconstructed global⁴⁷ and mid- to high-latitude Northern Hemisphere⁴⁸ atmospheric concentrations in the 1970s, at the peak of the anthropogenic pollution. Such concentrations, however, are unrealistic for the early Holocene, which implies that other drivers contributed to the enhancement of Hg during this period.

Another possible contributor to the Hg flux is FYSI, a known source of reactive Br during spring⁴⁹. The larger fraction of FYSI in the Arctic led to a greater fraction of gas-phase reactive Br transported to the EGRIP site at the onset of the Holocene, as indicated by our Br measurements (Fig. 1). Since oxidized Hg is more prone to surface deposition, atmospheric oxidation of Hg by Br causes enhanced deposition of Hg to the snow pack. Therefore, Arctic Br levels and Hg oxidation are ultimately dependent on the FYSI extent. To estimate the impact of atmospheric chemistry on the observed EGRIP Hg flux variability, we model atmospheric Hg oxidation reactions, considering the temperature effect on their kinetics. Br and Hg atmospheric budgets are considered in terms of relative changes, given that a large fraction of deposited Hg(II) is rapidly photo-reduced and re-emitted back to the atmosphere and that Hg accumulation rates in ice cores are proportional to atmospheric levels¹⁵. We find that enhanced atmospheric Hg oxidation by higher Br levels at the early Holocene leads to a greater Hg flux change. However, the simulation indicates that, if the Hg flux was controlled only by Br chemistry, total inorganic Br (Br₀) concentrations of ~22 pptv would be required to explain the threefold increase in Hg average deposition in the early Holocene compared with the Younger Dryas. These values are typically observed during spring bromine explosion events but are unlikely to be sustained year-round⁵⁰. From this, we conclude that higher Br concentrations during warm periods contributed to enhanced atmospheric Hg oxidation and deposition to the Arctic ecosystems during the early Holocene, but they are not the controlling factor.

After emissions and atmospheric chemistry, we can now evaluate the possible role of atmospheric transport and dust. Atmospheric Hg uptake on mineral dust was suggested as the main driver of Hg variability at Dome C in Antarctica during glacial periods, which were characterized by stronger winds and drier conditions, leading to higher atmospheric mineral dust loadings¹⁷. At EGRIP, elevated Ca fluxes during cold periods indicate greater transport of mineral dust to the site (Fig. 1)⁵¹. However, Hg and Ca fluxes show different trends and have no correlation during the Younger Dryas. Using the model to isolate the contribution of Hg uptake of dust, we find that the resulting Hg flux is indeed higher during cold periods and lower in warm periods, qualitatively similar to the results at Dome C¹⁷. Thus, the estimated Hg flux resulting from the contribution of dust uptake alone cannot explain the Arctic Hg variability observed in the Glacial–Holocene transition, but rather has a counteracting effect.

We therefore conclude that the most plausible explanation for the greater Hg fluxes recorded in the early Holocene is a combination

of enhanced Hg oceanic evasion to the atmosphere and enhanced Br-mediated Hg oxidation in the atmosphere, both influenced by climate-warming-induced sea-ice variability. Considering the relative change in EGRIP Br flux from the Younger Dryas to the early Holocene, our model further estimates that Br-mediated Hg oxidation accounts for a maximum of 25% of Hg flux, while the main driver is Hg evasion, accounting for a minimum of 75% (Supplementary Table 4). It is thus likely that the increased open ocean in the Baffin Bay and subpolar North Atlantic at the onset of the Holocene resulted in increased Hg evasion from the surface ocean and was the primary driver of the trend observed. The larger emission of reactive Br species from the larger FYSI fraction probably also contributed to the early Holocene signal.

Implications for future Arctic mercury

In this study, we reconstruct the Arctic mercury biogeochemical cycle for the period that covers the Glacial–Holocene transition. This research is contextualized in a new and rapid-growing field of investigation of reactive elements that, for their nature, have a strong impact in the environment, especially in a context of climate change. Past ice-core reconstructions over periods of abrupt climate variations are fundamental for estimating the main sources of these elements, as well as their impact on climate. In this context, our study sheds light on the variability of the Arctic mercury biogeochemical cycle in response to climate warming, along with potential implications for the near future. The EGRIP Hg high-resolution record shows that the biogeochemical cycle of Hg in the Arctic was highly sensitive to climate and, in particular, changes in sea-ice cover. The period investigated, the LGT and early Holocene (9.0–15.7 kyr b2k), is valuable for investigating the main natural sources of Hg since it covers a period of no anthropogenic influence. Our study suggests that Hg deposition in the Arctic increased at the onset of the Holocene driven by perennial sea-ice break-up and a larger area of ice-free ocean. This condition led to greater Hg evasion from the ocean and subsequent deposition to the surface of the Greenland Ice Sheet (Fig. 3).

In the context of current climate warming, progressive sea-ice decline and environmental change in the Arctic region, our results suggest a potential increase in oceanic Hg evasion in the near future. Most climate models predicted ice-free summer conditions in the Arctic Ocean by 2050 or earlier⁵², increase in marine productivity⁵³, increased glacier and permafrost melt and 3–4 °C warmer global temperatures with a three- to fourfold amplification in the Arctic by 2100 CE⁵⁴. Our study brings further evidence that natural sources of mercury may substantially contribute to the Hg inventory in the Arctic in the coming decades. To quantitatively evaluate the impact of climate change on the Arctic biogeochemical cycle, however, further studies are necessary.

Online content

Any methods, additional references, Nature Portfolio reporting summaries, source data, extended data, supplementary information, acknowledgements, peer review information; details of author contributions and competing interests; and statements of data and code availability are available at <https://doi.org/10.1038/s41561-023-01172-9>.

References

1. Dastoor, A. et al. Arctic mercury cycling. *Nat. Rev. Earth Environ.* **3**, 270–286 (2022).
2. Chételat, J. et al. Climate change and mercury in the Arctic: abiotic interactions. *Sci. Total Environ.* **824**, 153715 (2022).
3. AMAP Assessment 2021: Mercury in the Arctic (AMAP, 2021).
4. Amos, H. M. et al. Observational and modeling constraints on global anthropogenic enrichment of mercury. *Environ. Sci. Technol.* **49**, 4036–4047 (2015).
5. Krabbenhoft, D. P. & Sunderland, E. M. Global change and mercury. *Science* **341**, 1457–1458 (2013).

6. Amos, H. M., Jacob, D. J., Streets, D. G. & Sunderland, E. M. Legacy impacts of all-time anthropogenic emissions on the global mercury cycle. *Glob. Biogeochem. Cycles* **27**, 410–421 (2013).
7. Outridge, P. M., Mason, R. P., Wang, F., Guerrero, S. & Heimbürger-Boavida, L. E. Updated global and oceanic mercury budgets for the United Nations Global Mercury Assessment 2018. *Environ. Sci. Technol.* **52**, 11466–11477 (2018).
8. Obrist, D. et al. A review of global environmental mercury processes in response to human and natural perturbations: changes of emissions, climate, and land use. *Ambio* **47**, 116–140 (2018).
9. Mason, R. P. & Sheu, G.-R. Role of the ocean in the global mercury cycle. *Glob. Biogeochem. Cycles* **16**, 40–1 (2002).
10. Zaferani, S., Pérez-Rodríguez, M. & Biester, H. Diatom ooze—a large marine mercury sink. *Science* **361**, 797–800 (2018).
11. Driscoll, C. T., Mason, R. P., Chan, H. M., Jacob, D. J. & Pirrone, N. Mercury as a global pollutant: sources, pathways, and effects. *Environ. Sci. Technol.* **47**, 4967–4983 (2013).
12. Saiz-Lopez, A. et al. Photoreduction of gaseous oxidized mercury changes global atmospheric mercury speciation, transport and deposition. *Nat. Commun.* **9**, 4796 (2018).
13. Steffen, A. et al. A synthesis of atmospheric mercury depletion event chemistry in the atmosphere and snow. *Atmos. Chem. Phys.* **8**, 1445–1482 (2008).
14. Wang, K. et al. Subsurface seawater methylmercury maximum explains biotic mercury concentrations in the Canadian Arctic. *Sci. Rep.* **8**, 14465 (2018).
15. Kang, S. et al. Atmospheric mercury depositional chronology reconstructed from lake sediments and ice core in the Himalayas and Tibetan Plateau. *Environ. Sci. Technol.* **50**, 2859–2869 (2016).
16. Cooke, C. A., Martínez-Cortizas, A., Bindler, R. & Sexauer Gustin, M. Environmental archives of atmospheric Hg deposition—a review. *Sci. Total Environ.* **709**, 134800 (2020).
17. Jitaru, P. et al. Atmospheric depletion of mercury over Antarctica during glacial periods. *Nat. Geosci.* **2**, 505–508 (2009).
18. Pérez-Rodríguez, M., Horák-Terra, I., Rodríguez-Lado, L., Aboal, J. R. & Martínez Cortizas, A. Long-term (~57 ka) controls on mercury accumulation in the Southern Hemisphere reconstructed using a peat record from Pinheiro Mire (Minas Gerais, Brazil). *Environ. Sci. Technol.* **49**, 1356–1364 (2015).
19. Pérez-Rodríguez, M. et al. The role of climate: 71 ka of atmospheric mercury deposition in the Southern Hemisphere recorded by Rano Aroi Mire, Easter Island (Chile). *Geosciences* **8**, 374 (2018).
20. Schneider, L., Cooke, C. A., Stansell, N. D. & Haberle, S. G. Effects of climate variability on mercury deposition during the Older Dryas and Younger Dryas in the Venezuelan Andes. *J. Paleolimnol.* **63**, 211–224 (2020).
21. Roos-Barraclough, F., Martínez-Cortizas, A., García-Rodeja, E. & Shotyk, W. A 14 500 year record of the accumulation of atmospheric mercury in peat: volcanic signals, anthropogenic influences and a correlation to bromine accumulation. *Earth Planet. Sci.* **202**, 435–451 (2002).
22. Zheng, J. Archives of total mercury reconstructed with ice and snow from Greenland and the Canadian High Arctic. *Sci. Total Environ.* **509–510**, 133–144 (2015).
23. Pérez-Rodríguez, M. et al. Industrial-era lead and mercury contamination in southern Greenland implicates North American sources. *Sci. Total Environ.* **613–614**, 919–930 (2018).
24. Shotyk, W. et al. Anthropogenic contributions to atmospheric Hg, Pb and As accumulation recorded by peat cores from southern Greenland and Denmark dated using the ¹⁴C ‘bomb pulse curve’. *Geochim. Cosmochim. Acta* **67**, 3991–4011 (2003).
25. Zdanowicz, C. et al. Pre-industrial and recent (1970–2010) atmospheric deposition of sulfate and mercury in snow on southern Baffin Island, Arctic Canada. *Sci. Total Environ.* **509–510**, 104–114 (2015).
26. Cooke, C. A., Wolfe, A. P., Michelutti, N., Balcom, P. H. & Briner, J. P. A Holocene perspective on algal mercury scavenging to sediments of an Arctic Lake. *Environ. Sci. Technol.* **46**, 7135–7141 (2012).
27. Müller, J. & Stein, R. High-resolution record of late glacial and deglacial sea ice changes in Fram Strait corroborates ice–ocean interactions during abrupt climate shifts. *Earth Planet. Sci. Lett.* **403**, 446–455 (2014).
28. Werner, K. et al. Holocene sea subsurface and surface water masses in the Fram Strait—comparisons of temperature and sea-ice reconstructions. *Quat. Sci. Rev.* **147**, 194–209 (2016).
29. Gibb, O. T., Steinhauer, S., Fréchette, B., de Vernal, A. & Hillaire-Marcel, C. Diachronous evolution of sea surface conditions in the Labrador Sea and Baffin Bay since the last deglaciation. *Holocene* **25**, 1882–1897 (2015).
30. Hoff, U., Rasmussen, T. L., Stein, R., Ezat, M. M. & Fahl, K. Sea ice and millennial-scale climate variability in the Nordic Seas 90 kyr ago to present. *Nat. Commun.* **7**, 12247 (2016).
31. Spolaor, A. et al. Canadian Arctic sea ice reconstructed from bromine in the Greenland NEEM ice core. *Sci. Rep.* **6**, 33925 (2016).
32. Kindler, P. et al. Temperature reconstruction from 10 to 120 kyr b2k from the NGRIP ice core. *Climate* **10**, 887–902 (2014).
33. Fischer, H., Ruth, U. & Ro, R. Glacial/interglacial changes in mineral dust and sea-salt records in polar ice cores: sources, transport, and deposition. *Rev. Geophys.* **45** (2007).
34. Spolaor, A. et al. Halogen species record Antarctic sea ice extent over glacial–interglacial periods. *Atmos. Chem. Phys.* **13**, 6623–6635 (2013).
35. Vallenga, P. et al. Sea-ice reconstructions from bromine and iodine in ice cores. *Quat. Sci. Rev.* **269**, 107133 (2021).
36. Saiz-Lopez, A. et al. Photochemistry of oxidized Hg(I) and Hg(II) species suggests missing mercury oxidation in the troposphere. *Proc. Natl Acad. Sci. USA* **117**, 30949–30956 (2020).
37. Mason, R. P. & Sheu, G. Role of the ocean in the global mercury cycle. *Glob. Biogeochem. Cycles* **16**, 1093 (2002).
38. Ariya, P. A. et al. Mercury physicochemical and biogeochemical transformation in the atmosphere and at atmospheric interfaces: a review and future directions. *Chem. Rev.* **115**, 3760–3802 (2015).
39. Soerensen, A. et al. A mass budget for mercury and methylmercury in the Arctic Ocean. *Glob. Biogeochem. Cycles* **30**, 560–575 (2016).
40. Dimento, B. P., Mason, R. P., Brooks, S. & Moore, C. The impact of sea ice on the air–sea exchange of mercury in the Arctic Ocean. *Deep Sea Res.* **144**, 28–38 (2019).
41. Agather, A. M., Bowman, K. L., Lamborg, C. H. & Hammerschmidt, C. R. Distribution of mercury species in the Western Arctic Ocean (US GEOTRACES GN01). *Mar. Chem.* **216**, 103686 (2019).
42. Not, C. & Hillaire-Marcel, C. Enhanced sea-ice export from the Arctic during the Younger Dryas. *Nat. Commun.* **3**, 647 (2012).
43. Oksman, M. et al. Younger Dryas ice margin retreat triggered by ocean surface warming in central-eastern Baffin Bay. *Nat. Commun.* **8**, 1017 (2017).
44. Pienkowski, A. J. et al. Seasonal sea ice persisted through the Holocene Thermal Maximum at 80° N. *Commun. Earth Environ.* **2**, 124 (2021).
45. Briner, J. P. et al. Rate of mass loss from the Greenland Ice Sheet will exceed Holocene values this century. *Nature* **586**, 70–74 (2020).
46. Vandal, G. M., Fitzgerald, W. F., Boutron, C. F. & Candelone, J.-P. Variations in mercury deposition to Antarctica over the last 34,000 years. *Nature* **362**, 621–623 (1993).
47. Amos, H. M. et al. Observational and modeling constraints on global anthropogenic enrichment of mercury. *Environ. Sci. Technol.* **49**, 4036–4047 (2015).

48. Fain, X. et al. Polar firn air reveals large-scale impact of anthropogenic mercury emissions during the 1970s. *Proc. Natl Acad. Sci. USA* **106**, 16114–16119 (2009).
49. Saiz-Lopez, A. & von Glasow, R. Reactive halogen chemistry in the troposphere. *Chem. Soc. Rev.* **41**, 6448–6472 (2012).
50. Simpson, W. R., Brown, S. S., Saiz-Lopez, A., Thornton, J. A. & von Glasow, R. Tropospheric halogen chemistry: sources, cycling, and impacts. *Chem. Rev.* **115**, 4035–4062 (2015).
51. Schüpbach, S. et al. Greenland records of aerosol source and atmospheric lifetime changes from the Eemian to the Holocene. *Nat. Commun.* **9**, 1476 (2018).
52. Overland, J. E. & Wang, M. When will the summer Arctic be nearly sea ice free? *Geophys. Res. Lett.* **40**, 2097–2101 (2013).
53. Yool, A., Popova, E. E. & Coward, A. C. Future change in ocean productivity: Is the Arctic the new Atlantic? *J. Geophys. Res. Oceans* **120**, 7771–7790 (2015).
54. Miller, G. H. et al. Arctic amplification: can the past constrain the future? *Quat. Sci. Rev.* **29**, 1779–1790 (2010).
55. Andersen, K. K. et al. High-resolution record of Northern Hemisphere climate extending into the last interglacial period. *Nature* **431**, 147–151 (2004).
56. Gerber, T. A. et al. Upstream flow effects revealed in the EastGRIP ice core using Monte Carlo inversion of a two-dimensional ice-flow model. *Cryosphere* **15**, 3655–3679 (2021).

Publisher's note Springer Nature remains neutral with regard to jurisdictional claims in published maps and institutional affiliations.

Springer Nature or its licensor (e.g. a society or other partner) holds exclusive rights to this article under a publishing agreement with the author(s) or other rightsholder(s); author self-archiving of the accepted manuscript version of this article is solely governed by the terms of such publishing agreement and applicable law.

© The Author(s), under exclusive licence to Springer Nature Limited 2023

Methods

Ice-core analyses

Led by an international team, EGRIP began in summer 2015 with the intention of drilling through the North-East Greenland Ice Stream to reach 2,550 m depth. The drilling site is located at 75° 38' N and 35° 60' W at 2,708 m above sea level.

Here we present results from the chemical analyses performed on the EGRIP ice core, extending from 9.0 to 15.7 kyr b2k (1,036–1,406 m depth). EGRIP samples were collected from a continuous flow analysis system at the University of Bern and frozen immediately at a temperature of -20°C . They were then transported in a frozen state to Ca' Foscari University of Venice for preparation and analysis. In Venice, the sample preparation was performed in a class 1000 clean room laboratory, under class 100 laminar-flow benches.

Samples for Br, Na and Ca analysis were transferred to polypropylene vials pre-cleaned with ultra-pure water and dried under a laminar-flow hood. As Hg is volatile, a dedicated procedure is required to stabilize Hg in solution. Each vial for Hg analysis was conditioned with a solution of ultra-pure water and 2% supra-pure hydrochloric acid (HCl) to prevent contamination. The solution was left for one week, after which it was rinsed with ultra-pure water and dried in a class 100 laminar-flow clean bench. Each sample was then transferred to a clean vial and acidified with 2% ultra-pure commercially available doubly distilled low-mercury HCl to preserve the Hg content in the sample⁵⁷.

Total Hg, Br, Na and Ca were determined by Inductively Coupled Plasma Single Quadrupole Mass Spectrometry (ICP-SQMS, Thermo Scientific iCAP RQ ICP-MS)^{58,59}. The instrument was fitted with a high-sensitivity insert on the skimmer cone to maximize ion transmission from the plasma. As samples for Hg analysis require different uptake and wash times compared with samples for Br, Na and Ca analysis, two separate analysis methods were used. The Hg analysis was conducted in kinetic energy discrimination mode to ensure removal of possible polyatomic interferences. Since these are very rare in Antarctic ice samples, the instrumental tuning could be maximized for ion transmission and sensitivity⁵⁸. For both analyses, the concentrations were calculated from calibration curves derived from external standards and were blank corrected. Standard concentrations ranged from 1 to 20 pg g^{-1} for Hg, from 1 to 200 ng g^{-1} for Na and Ca and from 0.01 to 2.00 ng g^{-1} for Br. The limit of detection of Hg analysis, calculated as 3.3 times the standard deviation of the blanks, was 0.20 pg g^{-1} . The instrumental relative standard deviation was stable through the analysis and showed levels $\leq 15\%$. Procedural blanks were obtained from the measurement of ultra-pure water acidified with 2% ultra-pure HCl and had an average concentration of 0.28 pg g^{-1} . Reproducibility was estimated to be -14% and was evaluated by reanalysing 13 selected samples, as well as by checking samples created by uniting aliquots of 5 samples into 1 vial. To evaluate Hg analysis accuracy by ICP-MS, an interlaboratory comparison was conducted with cold-vapour atomic fluorescence spectroscopy at the University of Manitoba, showing a 16% difference with respect to the ICP-MS measure (Supplementary Information). The measurements of Br, Na and Ca had limits of detection of 0.06 ng g^{-1} , 1.2 ng g^{-1} and 4.5 ng g^{-1} , respectively. To evaluate the repeatability, a sample with a known concentration was measured every 30 samples, resulting in a repeatability of -10% , -4% and -6% for Br, Na and Ca. Two sequences of analysis were dedicated to repeating the measurement of samples to further check the repeatability, resulting in more than 250 repeated samples.

The EGRIP age scale is published in ref. 60. Samples for Br, Na and Ca analysis cover a depth of 55 cm (bag) and have a resolution from -6 years in the upper part of the profile to -17 years in the bottom part. Samples for Hg analysis cover a depth of 1.65 m and -20 years for the upper part while for the bottom part, the resolution is 1.1 m depth and -36 years.

Hg, Br, Na and Ca can be deposited through wet and dry deposition; we calculate deposition fluxes to account for differences in

accumulation over time. We calculate fluxes ($\text{ng m}^{-2}\text{ yr}^{-1}$) by multiplying the element concentration by the accumulation rate (m yr^{-1} in water equivalent). The accumulation model is published in ref. 56.

Bromine enrichment (Br_{enr}) is employed in the study as a proxy of seasonal sea ice³¹. It is calculated as $\text{Br}_{\text{enr}} = \frac{[\text{Br}]_{\text{ice}}}{[\text{Na}]_{\text{ice}} \times 0.0062}$, where 0.0062 is the bromine/sodium concentration ratio in seawater.

Modelling approach

We use a photochemical box model to understand the driving factors of the abrupt changes between the observed Hg depositional flux during the Younger Dryas (11.7–12.9 kyr b2k) and early Holocene (9.0–11.7 kyr b2k). The model is based on the latest Hg chemical scheme^{36,61,62} and constrained according to various climatic parameters for the two periods (see Supplementary Information section 5 for details and the chemical scheme). We have used EGRIP ice-core Hg and Br average fluxes in the early Holocene and Younger Dryas to constrain relative changes in the deposition. Atmospheric Hg concentrations are ascribed according to reconstructions of Hg⁰ pre-industrial levels⁶³. We made several sensitivity tests to quantify the total impact of dust and bromine oxidation chemistry on the deposition rates, the results of which are detailed in the manuscript.

Data availability

EGRIP ice-core data are available in the Zenodo dataset (<https://zenodo.org/record/7754371>) and as Supplementary Data to this article.

Code availability

All files related to the box model are available at the following link: https://github.com/deliasegato1/box_model_EGRIP_Hg.git.

References

- Parker, J. L. & Bloom, N. S. Preservation and storage techniques for low-level aqueous mercury speciation. *Sci. Total Environ.* **337**, 253–263 (2005).
- Planchon, F. A. M. et al. Direct determination of mercury at the sub-picogram per gram level in polar snow and ice by ICP-SFMS. *J. Anal. At. Spectrom.* **19**, 823–830 (2004).
- Spolaor, A. et al. Diurnal cycle of iodine, bromine, and mercury concentrations in Svalbard surface snow. *Atmos. Chem. Phys.* **19**, 13325–13339 (2019).
- Mojtabavi, S. et al. A first chronology for the East Greenland Ice-core Project (EGRIP) over the Holocene and Last Glacial Termination. *Climate* **16**, 2359–2380 (2020).
- Francés-Monerris, A. et al. Photodissociation mechanisms of major mercury(II) species in the atmospheric chemical cycle of mercury. *Angew. Chem. Int. Ed.* **59**, 7605–7610 (2020).
- Shah, V. et al. Improved mechanistic model of the atmospheric redox chemistry of mercury. *Environ. Sci. Technol.* **55**, 14445–14456 (2021).
- Enrico, M. et al. Holocene atmospheric mercury levels reconstructed from peat bog mercury stable isotopes. *Environ. Sci. Technol.* **51**, 5899–5906 (2017).

Acknowledgements

EGRIP is directed and organized by the Centre for Ice and Climate at the Niels Bohr Institute, University of Copenhagen. It is supported by funding agencies and institutions in Denmark (A. P. Møller Foundation, University of Copenhagen), USA (US National Science Foundation, Office of Polar Programs), Germany (Alfred Wegener Institute, Helmholtz Centre for Polar and Marine Research), Japan (National Institute of Polar Research and Arctic Challenge for Sustainability), Norway (University of Bergen and Trond Mohn Foundation), Switzerland (Swiss National Science Foundation), France (French Polar Institute Paul-Emile Victor, Institute for Geosciences and Environmental research), Canada (University of Manitoba) and

China (Chinese Academy of Sciences and Beijing Normal University). A.S. acknowledges the 'Programma di Ricerca in Artico' (PRA, project number PRA2019-0011, Sentinel) for supporting this work. A.S.-L. received funding from the European Research Council Executive Agency under the European Union's Horizon 2020 Research and Innovation Programme (project ERC-2016-COG 726349 CLIMAHAL). This work represents a contribution to CSIC Thematic Interdisciplinary Platform PTI POLARCSIC. A.S.M. acknowledges the Indian Institute of Tropical Meteorology (IITM), funded by the Ministry of Earth Sciences (MOES), Government of India (GOI). F.W. received funding from the Canada Research Chairs Program. T.E., C.M.J. and C.Z. acknowledge the long-term support of ice-core research by the Swiss National Science Foundation (SNSF) under the project numbers 200020_172506, 200020B_200328 and 20FI21_164190 as well as the Oeschger Center for Climate Change Research. H.A.K. received funding from the DFF Inge Lehmann grant 1131-00007B 'Holocene sea ice variability in the Arctic'. ELGA LabWater, High Wycombe, UK, supplied the pure-water system used in this study.

Author contributions

A.S., D.S. and A.S.-L. designed the study. D.S., C.T. and W.R.L.C. performed the Hg, Br, Na and Ca analyses. A.S.M. and D.S. performed the box model simulations. C.Z., T.E. and C.M.J. provided the EGRIP

dust profile. A.S.M., J.P.C. and F.W. contributed to the interpretation of the results. D.S., A.S.M., A.S.-L., A.S., F.W., J.P.C., W.R.L.C. and T.E. wrote the original manuscript. C.A.C., T.E., C.M.J., C.Z., W.R.L.C., H.A.K. and C.B. contributed to the review and editing of the manuscript. All authors provided input for the manuscript.

Competing interests

The authors declare no competing interests.

Additional information

Supplementary information The online version contains supplementary material available at <https://doi.org/10.1038/s41561-023-01172-9>.

Correspondence and requests for materials should be addressed to Alfonso Saiz-Lopez or Andrea Spolaor.

Peer review information *Nature Geoscience* thanks Giovanni Baccolo and the other, anonymous, reviewer(s) for their contribution to the peer review of this work. Primary Handling Editor: James Super, in collaboration with the *Nature Geoscience* team.

Reprints and permissions information is available at www.nature.com/reprints.